THERMORESPONSIVE *IN-SITU* GELLING OPHTHALMIC DRUG DELIVERY SYSTEM BASED ON XYLOGLUCAN CONTAINING TRIAMCINOLONE ACETONIDE NANOPARTICLES

YOGESH A. SONAR and HITENDRA S. MAHAJAN

Department of Pharmaceutics, R. C. Patel Institute of Pharmaceutical Education and Research, Shirpur 425405, Maharashtra, India

™ Corresponding author: H. S. Mahajan, hsmahajan@rediffmail.com

Received April 25, 2025

This investigation explores the feasibility of using a gel formulation composed of xyloglucan for the administration of triamcinolone acetonide (TA) nanoparticles in ophthalmic drug delivery systems. The solvent evaporation method with lyophilization was employed to develop TA-loaded β -cyclodextrin (β CD)-Soluplus (Solu) nanoparticles (NPs), which were subsequently optimized using the response surface methodology (central composite design, CCD), indicating that the independent variables had a significant impact on particle size and percentage encapsulation. In addition to solid-state assessment using FTIR, XRD, DSC, and surface properties using scanning and transmission electron microscopy (SEM and TEM), the developed nanoparticles were confirmed to have a nanospherical structure and a stable formulation. The release profile and *in vitro* and *ex vivo* assessments were utilized to evaluate the drug discharge mechanisms of the developed formulation, which showed prolonged release for 8 h. The optimized formulation exhibited improved corneal permeation compared to the pure drug and showed no irritancy, as evidenced by the HET-CAM test.

Keywords: in situ gel, xyloglucan, triamcinolone acetonide, HET-CAM, ocular drug delivery, nanoparticles

INTRODUCTION

An eye is an organ that is both compact and complex. It consists of two separate sections, anterior and posterior. The cornea, crystalline lens, conjunctiva, iris, ciliary body, and aqueous humor constitute the anterior portion of the eye. By contrast, the choroid, retinal pigment epithelium, and sclera comprise the posterior region. Many people worldwide are affected by ocular problems, which directly affect their vision and general quality of life. Cataracts, dry eye conditions (DES), macular degeneration caused by age (AMD), glaucoma, inflammation of the eye, retinopathy due to diabetes (DR), and retinal vein blockages (RVO) are the main disorders that impair vision. Except for cataracts, which require surgery to remove the hazy lens and replace it with a synthetic lens, most of these conditions are managed with medicine.1-4

Intravitreal injections are frequently used to treat problems of the posterior segment, whereas eye drops are usually administered directly to the afflicted area to treat diseases of the anterior segment. The small size of the ocular cavity, system of nasolacrimal drainage, processes of precorneal elimination, conjunctival uptake, and short retention time all hinder the availability of active ingredients at the specific site and their potential therapeutic effects. While intravitreal injections can deliver a consistent dose to enhance drug absorption in the eye, they must be administered as infrequently as possible to limit the overall number of injections because patients experience discomfort from frequent intraocular injections and run the risk of developing retinal detachment and endophthalmitis. 5-7

In recent years, numerous delivery systems have been developed, including the application of prodrugs, penetrators, *in situ* gels, and vehicles for the delivery of drugs, such as liposomes, niosomes, microneedles, nano- or microparticles, and dendrimers, to prolong ocular retention, improve penetration of the drug through ocular obstructions, and enhance bioavailability.^{8–11}

Currently, the number of in situ forming mechanisms has increased and has documented before tissue repair. Aqueous polymeric solution in situ gelling systems transform into gels because of variations in various conditions, such as temperature range, concentration, and pH. Liquids known as "in-situ gels" are capable of entering the body using a less invasive procedure and solidifying or hardening inside the targeted area.^{8–10,12–14} Removal of over 35% residual galactose from xyloglucan using βgalactosidase results in thermoresponsive reversible gel formation in a dilute aqueous solution, thereby rendering it a thermally responsive material. This investigation explored the feasibility of employing a gel formulation comprising a xyloglucan polysaccharide for the administration of triamcinolone acetonide in ophthalmic drug delivery systems, as reported in previous studies. 14-17 Triamcinolone acetonide is an artificial glucocorticoid (TA) immunomodulatory and anti-inflammatory characteristics. It is extensively utilized as a costeffective remedy for several eye conditions. Several commercially available formulations of injectable TA have been considered off-label ophthalmic treatments that can be administered via sub-tenon injections or intravitreal injections for treating various chorioretinal diseases. 4,7,11,18

This study involves the creation of an ocular in situ gel utilizing xyloglucan, a temperatureresponsive polymer that incorporates triamcinolone acetonide. The nanoparticles were fabricated using a solvent evaporation method, beta-cyclodextrin and Soluplus encapsulate the drug. The dry nanoparticles were collected after lyophilization. The optimization was performed with the help of Quality by Design by employing a central composite design (CCD), focusing on the size of the nanoparticles and polydispersity index (PDI). The developed nanoparticles were evaluated for their solid-state characteristics after *in vitro* and *ex vivo* release in simulated tear fluid. *In situ* gelling was achieved using an in-house developed raw xyloglucan for thermoresponsiveness. Finally, the chorioallantoic membrane test, often known as Hen's egg test, was used to conduct the ocular irritancy study (HET-CAM test). ^{19–22}

EXPERIMENTAL

Materials

Amneal Pharma Pvt. Ltd., Ahmadabad, provided a gift sample of triamcinolone acetonide (TA), DSP Gokyo Food and Chemical Co. Ltd. (Fukusima, Japan) produced xyloglucan from tamarind seeds, Sigma Aldrich Ltd. provided *Aspergillus oryzae* β -galactosidase and β -cyclodextrin (β CD) (purchased), HiMedia India sold galactose, and BASF India (Turbhe, Thane) gave a gift of Soluplus (Solu), all of which were of analytical grade and used as received.

Methods

TA loaded βCD-Solu nanoparticles (NPs) preparation

The solvent evaporation method was employed to formulate TA-loaded βCD-Solu nanoparticles, which were then improved by employing a software (Design-Expert)-assisted Central Composite Design (CCD). The responses selected were: particle measurement (size in nm) and drug entrapment rate (% EE), which were paired with the independent variables: βcyclodextrin (βCD) and Soluplus (Solu) content (Table 1). The factors and responses, along with their evaluation ranges, are outlined as per the CCD parameters. Different quantities of BCD-Solu were prepared by dissolving various quantities, as specified by the CCD, in distilled water (50 mL) while stirring magnetically using a stirrer (Solution A). 50 millilitres of acetone (Solution B) were used to homogenize the pure drug TA. Next, solution B was gradually added to solution A at a rate of 1 mL per minute, while using a High-Speed Homogenizer (IKA ULTRA-TURRAX T 25, Germany) set to 5,000 rpm. Once the addition was complete, the speed was increased to 10,000 rpm for 10 min.

Table 1
Independent and dependent variables with experimental ranges as per CCD design

Variables	Units	Levels used for coding			
Factors (independent)		-1	0	+1	
$A = \beta$ cyclodextrin (β CD)	mg	56.75	113.5	170.25	
B = Soluplus (Solu)	mg	29.47	35.36	41.26	
Responses (dependent)	-	Constrain			
R1 = PS	d. nm	In range			
R2 = EE	%	Maximum			

^{*}A and B = factors, R1 and R2 = responses, PS = particle size, EE = entrapment efficiency, d nm = diameter in nanometers, -1 = low, 0 = middle, and +1 = high levels

After homogenization, the mixture was allowed to remain on a magnetic stirrer overnight at ambient temperature to completely remove the organic phase (acetone).

The resulting dispersion was then lyophilized at -50 °C using a Vir-Tis freeze dryer (SP Scientific, USA) to obtain a powder form. Several parameters were examined to analyze the physical properties of the produced nanoparticles, several parameters were examined. ²³⁻²⁶

Development of thermo-responsive xyloglucan for insitu gelation

Xyloglucan, with a 45% reduction in galactose, was produced through enzymatic degradation of tamarind seed xyloglucan, following a previously described methodology. 13-14 To eliminate the specified quantity of β-D-galactose residues, the Aspergillus oryzae enzyme β-galactosidase (8.0 U/mL) was added to a 2.0% xyloglucan water solution. The reaction was continued for 24 h at 30 °C with a pH of 4.5. The sample was then heated for 20 min at 100 °C to deactivate the enzyme. The xyloglucan that had been degraded by the enzyme was collected by adding ethanol to precipitate it from the solution, washed with water three times, and the resulting product was dried at 60 °C. The HPTLC made by CAMAG, Muttenz Switzerland (applicator – Linomat 5, automatic development chamber - CAMAG ADC2, TLC scanner - CAMAG 3, and WinCATs v 1.4.10 data processor) was used to determine the galactose content of the collected supernatant at the time of purification. The galactose removal ratio (GRR) was calculated by:

$$GRR = \frac{Galactose\ residue\ (Released)}{Galactose\ Residue\ (Total)} \times 100 \tag{1}$$

The total galactose residue was quantified following complete hydrolysis by heating the collected sample with 2N $\rm H_2SO_4$ at a temperature of 100 °C for three hours. $^{14-16}$

Characterization

Physicochemical analysis of TA-loaded β CD-Solu-NPs

Surface morphology study

The surface morphology was examined by scanning and transmission electron microscopy (SEM and TEM, respectively). For SEM examination, gold powder was applied by spraying onto the formulation, which was affixed to a sample holding plate using adhesive tape. The sample was examined morphologically using a scanning electron microscope (JEOL/EO model JSM-6390LV, JEOL, Tokyo, Japan) at a voltage of 15 kV, both before and following mechanical activation.²⁹ The TEM system (Jeol/JEM 2100), with a lattice spacing of 0.14 nm, a resolution point of 0.23 nm, and an acceleration voltage of 200 kV, was employed for further surface characterization of the nanoparticles. A single drop was applied to a copper grid to create nanoparticle samples, which were subsequently vacuum-dried. Before examination, the dried nanomaterials were dyed for 30 s with 1% phosphor-tungstic acid solution.^{21,30}

Estimation of formulated nanoparticle's size and surface charge

The average nanoparticle size, polydispersity index (PDI), and surface charge were evaluated using a ZS90 Zetasizer (Malvern brand, UK). A 1:10 dilution ratio was used for the samples in water with zero dissolved solids (0 TDS water) to achieve optimal particle counts. The assessment was performed at ambient temperature with a diffraction angle of 90°and an electric field of 25 Vm⁻¹.^{21–23}

Entrapment efficiency (% EE)

An Optima Max-XP ultracentrifuge (Cooling centrifuge; Beckman Coulter, Switzerland) was used to ultracentrifuge the resultant nanosuspension for 20 min at a rate of 50,000 rpm. A Shimadzu UV-visible spectrophotometer (1700, Shimadzu®, Tokyo, Japan) was used to measure the absorbance at λmax = 238 nm to determine the free drug concentration (TA). The total quantity of TA used was subtracted from the quantity of free TA present in the aliquot to calculate the percentage of entrapment efficiency (% EE). An R² value of 0.9989 was obtained by repeating the measurements thrice and using a linear equation to determine the percentage of encapsulation. ^{21,27-28}

$$y = 0.0197x + 0.0275$$
Entrapment Efficiency (%) =
$$\frac{\text{Total quantity of the TA - Quantity of TA in supernatant}}{\text{Total quantity of the TA}} \times 100$$
(3)

Dry-state estimation of TA-loaded \$CD-Solu-NPs

Fourier transform infrared spectroscopy (FTIR)

The infrared spectra for TA, excipients, physical mixture, and the optimized formulation were recorded using an FTIR coupled with an Attenuated Total Reflectance (ATR) spectrophotometer (Bruker Alpha II, Germany). Infrared spectra were gathered between 4000 and 400 cm⁻¹. ³¹⁻³³

X-ray diffractometry analysis (XRD)

X-ray diffraction (XRD) of TA, blank nanoformulation, and TA-loaded NPs was performed using an X-ray diffractometer (Bruker D2 Phaser $2^{\rm nd}$ generation, Germany) at 30 kV and 10 mA. Every sample was examined at an angle of 2θ , ranging from 5 to 50 degrees, and an angular increment of 0.3 degrees per second.

Differential scanning calorimetry (DSC) assessment

The heat responses of nanoparticles (NPs) were assessed using differential scanning calorimetry. A DSC (DSC 2, Mettler Toledo, India) was used to assess the physical mixture, TA-loaded β CD-Solu-NPs, and thermal properties of TA. An aluminum pan

was filled with samples weighing two–five milligrams, and an empty pan was used for comparison. Both pans were subjected to temperatures (30–350 °C) at a heating rate of 10 °C/min, while nitrogen gas was continuously purged at 50 mL/min flow rate.²¹⁻²²

Release assessment – in-vitro study

A modified Franz diffusion cell with a 12.5 mL capacity and an internal diffusion area of 3.11 cm² was employed to determine how TA diffused through the formulated batch. As a semi-permeable barrier, the dialysis membrane used in this modified diffusion cell had a molecular weight cut-off of 12-14 kDa. Both the improved formulations (TA-loaded βCD-Solu-NPs) and the pure medication were individually placed in the donor compartment. The receptor chamber was maintained at 35 ± 0.5 °C at 50 rpm using simulated tear fluid (STF-7.4 pH). Before analysis using HPLC (1100-Agilent Tech with auto-injector, C18 Agilent stationary phase, and Chemstation 10.1 software), 0.5 mL of STF was withdrawn from the receiver chamber at predefined intervals. To maintain the concentration gradient, an equal quantity of fresh STF was added.4,11,21

Drug diffusion kinetics

The findings from the release profile studies were utilized to illustrate the release mechanisms of the TA-loaded β CD-Solu-NPs formulation. The slope was used to obtain the release exponent (n) and kinetic constant (K):

$$Mt/_M = Ktn$$
 (4) where (n) is the exponent of release, (Mt) is the drug

released with respect to time (t), (M) is the overall drug release over an indefinite period, and (K) is the diffusional constant of the drug-polymer system.

If (n = 0.5), the mechanism of the release follows Fickian diffusion; if (n < 0.5), it indicates quasi-Fickian diffusion; while (n) values between 0.5 to 1.0 represents non-Fickian diffusion. When (n = 1), non-Fickian case II diffusion was present, whereas (n > 1.0) is an example of non-Fickian super case II diffusion. 23 -

Release assessment – ex-vivo permeation

For the *ex vivo* release estimation, an excised goat eyeball from a nearby market (slaughterhouse) was used. The donor compartment was then fastened to the cornea. An overall 3.11 cm² of the surface area was exposed by this donor chamber. The STF was used to dilute the optimized formulation and pure medication to reach the final TA concentration before they were placed in the donor compartment. The temperature was maintained at 35 °C \pm 0.5 °C, while the magnetic stirrer ran continuously at 50 rpm. Aliquots (0.5 mL) were removed and replaced with an equivalent amount of a new STF at predetermined intervals. The developed HPLC method was used to quantify the amount of released TA. 10,35

Thermal gelation (in-situ)

The specific sol-gel conversion temperature, defined as the gel formation temperature (GFT), was assessed using the tube-inversion technique. The 1 mL sample was kept at 4 °C in tiny glass vials with an internal diameter of approximately 10–15 mm. It was then heated at 1 °C/min in a thermocontrolled water bath that ranged from 5 to 50 °C. The gel formation temperature (GFT) was measured as the temperature at which the liquid within the tube became viscous within 30 s. ^{14,36} A Brookfield DV-E viscometer (Brookfield Engineering Laboratories, Inc., USA) was used to test viscosity.

Hen's egg test – chorioallantoic membrane study (HET-CAM test)

Fresh viable eggs weighing between 50.0 to 60.0 g were sourced from native farmers. Before conducting the tests, the eggs were carefully inspected for imperfections or anomalies. The eggs were stored at 37.8 ± 0.30 °C with 58.2% relative humidity (% RH) in the incubator. During the 8-day incubation period, each egg was rotated five times per day. On day nine, each egg was removed from the incubator. The outer shells of the eggs were removed gently without damaging the inner layer. 0.5 mL of the optimized formulation comprising TA-loaded βCD-Solu-NPs was applied to the exposed CAM, and 0.9% NaCl (negative reference) and 0.1 N NaOH (positive reference) were applied separately. At intervals of 0.5, 2, and 5 min, the blood vessels and a network of capillaries were inspected for coagulation, hemorrhage, and hyperemia. Each test's findings were noted, and categorization was performed by employing an average result similar to the Draize categorization. 23,37

Statistical analysis

Statistical analysis was performed using the Origin software (OriginLab Corporation, Northampton, MA, USA). ANOVA (One-way analysis of variance) was used to compare several groups. Statistical significance was set at p < 0.05. All experimental data are displayed as mean \pm standard deviation (SD) derived from at least three measurements for each trial.

RESULTS AND DISCUSSION

The primary objective of this study was to develop and assess TA-loaded β CD-Solu-NPs by solvent evaporation. The aim was to create a stable thermo-responsive formulation that enhances corneal permeation, which was further optimized using a Quality by Design (QbD) strategy. The QbD enables the collection of statistical feedback regarding both factors and responses. The requirements of the drug delivery methods fulfilled by varying ratios of β CD and Solu were examined as material factors at different concentrations, representing an outcome-

driven assessment pertinent to drug encapsulation

and particle size (Table 2).

Table 2							
Batchwise observed responses (dependent variables))						

Run no.	βCD A (mg)	Soluplus B (mg)	Particle size (d. nm)	Encapsulation EE (%)
1	0	0	145.2	84.32
2	+1	+1	294.43	73.4
3	-1	-1	224.97	67.78
4	+1	-1	125.5	88.14
5	0	0	144.7	84.64
6	0	0	143.5	84.97
7	-1	+1	174.5	61.08
8	0	+1>	218.5	68.41
9	+1>	0	244.4	81.11
10	0	0	144.7	85.1
11	0	0	143.9	85.06
12	0	-1<	130	83.5
13	-1<	0	228.44	58.1
OF	126.27	34.92	144.7 ± 3.1	$84.37 \pm 2.1\%$

*OF = optimized formulation (based on the desirability of 1 - numerical method), > & < = more than and less than coded levels (n = 3 times)

Optimization of formulation using DoE

Central composite design (CCD) was used to determine how independent factors influenced the dependent responses. The concentrations of β CD and Solu were taken as material factors, while the encapsulation drug (% EE) and particle size (PS d.nm) were designated as responses. The impact of these factors on the responses was analyzed by composing equations with polynomials and response graphs (contour and 3D surface plots). The expression for the polynomial equations for replies (Y1) and (Y2): PS = 1325.4 + -8.93797 * A + -43.5738 * B +

$$0.163956 * AB + 0.0142487 * A^2 + 0.425995 * B^2$$
 (5)
% EE = -115.237 + 0.895452 * A + 8.88598 * B + -0.00600823 * AB + -0.00237583 * A^2 + -0.128816 * B^2 (6)

Equation (5) states that components A and B have antagonistic effects on the particle size, as indicated by their negative coefficients of -8.93797 * A and -43.5738 * B, respectively. Conversely, Equation (6) indicates a positive correlation between the independent variables and percentage drug entrapment, demonstrating a synergistic effect from independent factor A (β CD) and an additive effect from factor B (amount of Solu), as indicated by +0.895452 * A and + 8.88598 * B in Equation (6). The model equations proposed by Design Expert reflected high R² values of 0.9998 and 0.9996 for Y1 (PS) and Y2 (EE), respectively, illustrating a strong linear relationship between the chosen variables.

The p-values for Y1 and Y2 were 0.0001 (Tables 3 and 4) and the equations with the model were quadratic and significant (p-0.05). The experimental results demonstrated that the material factors had a substantial effect on the % encapsulation and particle size.

Tables 3 and 4 present the ANOVA results for Y1 and Y2 models, which show that drug encapsulation was significantly influenced (p<0.0001) by the interaction between β-CD and (A and B) concentrations. Factors A, B, and B² were identified as critical terms in the statistical analyses. The model was further validated using an F-value of 5735.29, indicating the statistical relevance of the model terms. Furthermore, the discrepancy between the anticipated R² (0.9986) and Adjusted R² (0.9996) values was less than 0.2. A p-value of less than 0.0500 for response Y2 reiterated the statistical importance of the model terms. The characterization correlations for A, B, and B2 confirmed a close relationship and direct influence on response Y2, with an F-value of 3489.63, highlighting statistical model significance. Again, the difference of 0.2 between the anticipated R^2 (0.9991) and the adjusted R^2 (0.9993) indicated minimal variation between the predicted and experimental data during statistical assessment.

3D response graphs visually illustrate the response values, serving as a critical tool for discerning the primary and interaction effects of the independent variables. These plots assessed

how the independent factors affected the dependent outcomes (Y1 and Y2).

Table 3 ANOVA overview of particle sizes of the prepared nanoparticles

Source	Obtained F-value	Obtained p-value	Significance
Model	5735.29	< 0.0001	Significant
Lack of fit	4.71	0.0844	Non-significant
A-βCD	190.27	< 0.0001	
B-Soluplus	6098.66	< 0.0001	
AB	9892.80	< 0.0001	
A^2	12042.33	< 0.0001	
\mathbf{B}^2	1253.26	< 0.0001	

Table 4 ANOVA overview of entrapment efficiency of the prepared nanoparticles

Source	Obtained F-value	Obtained p-value	Significance
Model	3489.63	< 0.0001	Significant
Lack of fit	0.2070	0.8868	Non-significant
A-βCD	7307.75	< 0.0001	_
B-Soluplus	3144.12	< 0.0001	
AB	222.10	< 0.0001	
A^2	5597.36	< 0.0001	
B^2	1915.87	< 0.0001	

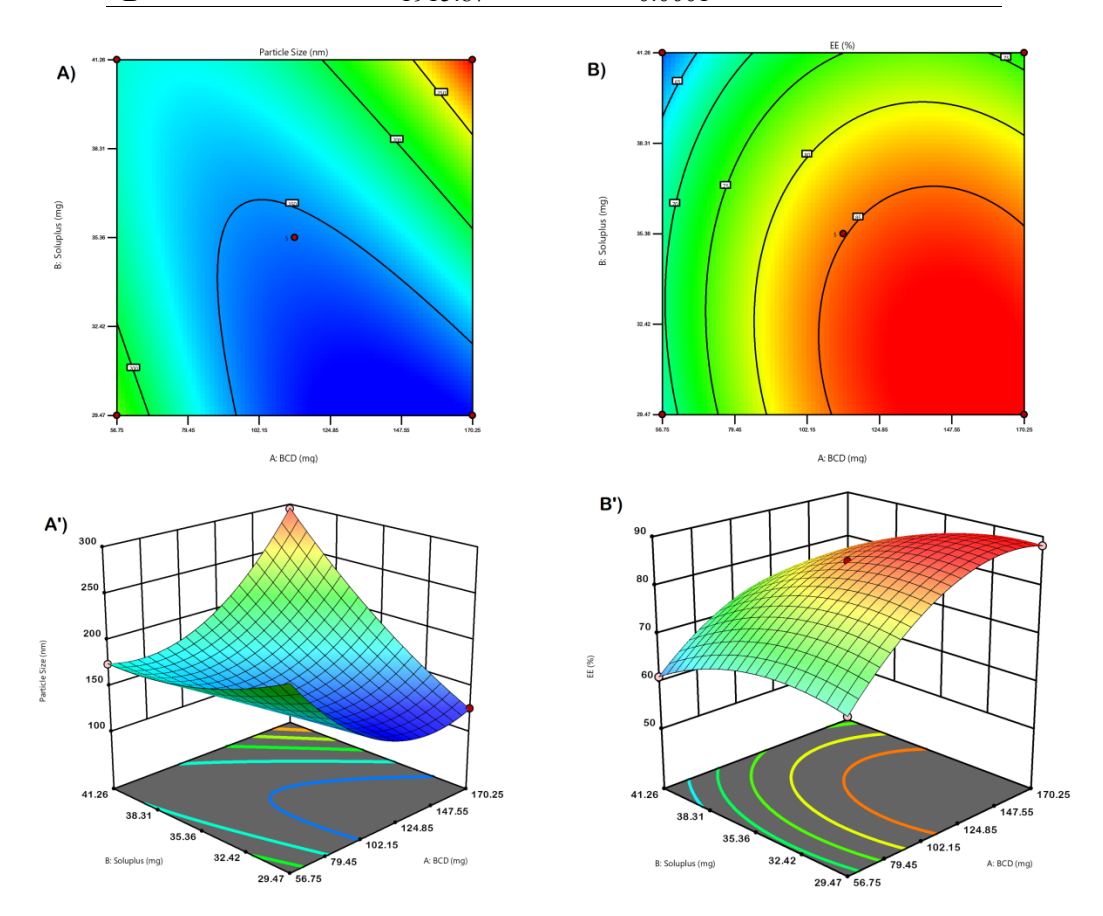


Figure 1: Contour plots (A) and (B), and 3D graphs (A') and (B') displaying the impact of βCD and Soluplus on the particle size and encapsulation ability, respectively

The % of encapsulated drug and the impact of βCD and Solu on nanoparticle size are presented in Figure 1, showing contour and 3D response surface graphs. The complete analysis outlines the optimization level attainable from the experimental values within the plots for the desired release outcomes.²³⁻³⁴

Galactose estimation by HPTLC

A novel, straightforward, and rapid HPTLC approach was employed for the quantitative estimation of galactose. ¹⁴ The method yielded a galactose spot (Rf = 0.69 ± 0.02) using a concentration between $2.00-10.00 \mu g/mL$, and a regression study of calibration plots demonstrated a good linear association with (R² = 0.9981). This method exhibited precision, accuracy, reproducibility, and selectivity for galactose analysis, with the galactose removal ratio (GRR) measured at 45.26%.

Physicochemical analysis of TA-loaded βCD-Solu-NPs

Surface morphology study

The surface properties of TA-loaded βCD-Solu-NPs prepared by solvent evaporation were examined using SEM and transmission electron

microscopes. Figure 2A presents an SEM image of TA-loaded β CD-Solu-NPs, which appeared spherical with sizes ranging from 150 to 180 nm. In comparison with the Zetasizer results, the diameter observed via SEM was slightly larger, likely due to the aggregation of particles during drying conditions. The HR-TEM image in Figure 2B confirms the spherical morphology.

Estimation of formulated nanoparticle size and surface charge

Dynamic light scattering (DLS) was used to analyze all prepared batches of nanoparticles to determine the particle size distribution. The optimized formulation batch containing TAloaded βCD-Solu-NPs was assessed for particle size by employing DLS and was found to have 144.7 \pm 3.1 d.nm particle size and PDI of 0.266 \pm (optimized formulation) (Fig. Measurements such as PDI and zeta potential offer an initial assessment of the nanoformulation stability. A PDI value below 0.3 indicates monodispersibility. The TA-loaded βCD-Solu-NPs exhibit a negative surface charge of -19.9 \pm 4.1 mV, suggesting the prepared nanocarrier dispersion is stable (Fig. 2D).

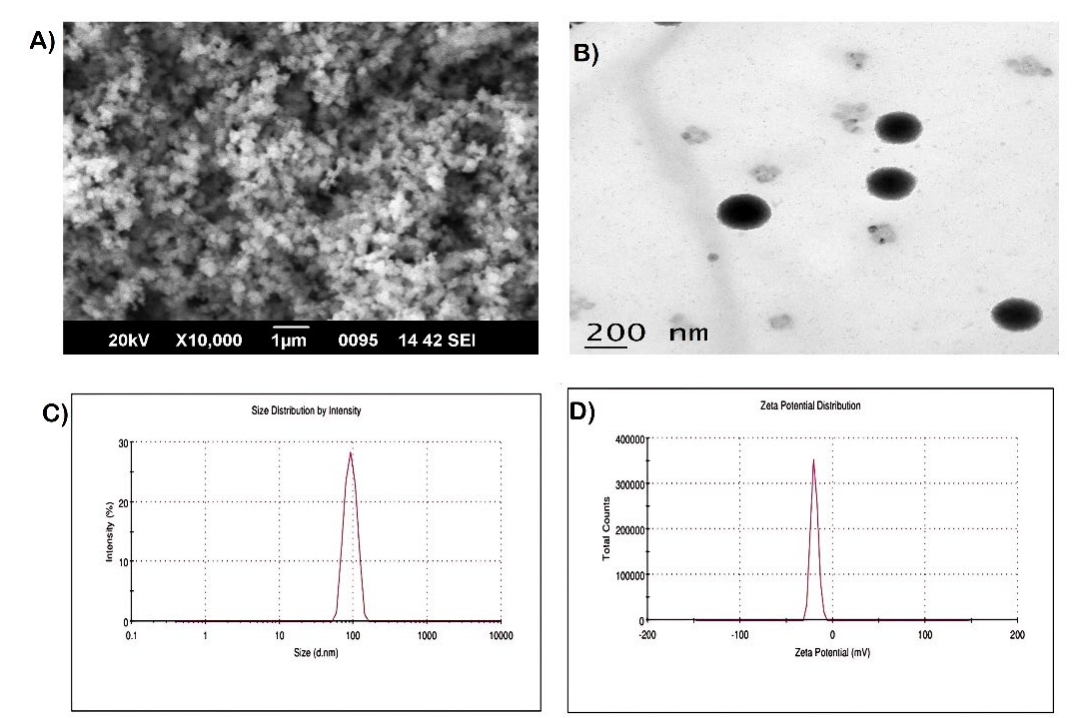


Figure 2: A) SEM image, B) TEM image, C) particle size distribution, and D) surface charge (zeta potential) distribution of TA-loaded βCD-Solu-NPs

Because DLS captures average particles in a hydrated condition, the HR-TEM observed

diameters were smaller than those determined by DLS and SEM measurements, most likely

because of particle contraction during sample preparation.

Entrapment efficiency (% EE)

The entrapment efficiency (% EE) of TA-loaded β CD-Solu-NPs complexes was determined to be 84.37 \pm 2.1% (optimized formulation obtained based on desirability 1 from applied CCD). The inclusion of cyclodextrin enhanced encapsulation, which was attributed to increased drug homogenization and stability of nanoparticles because of the presence of cyclodextrin and Soluplus.

Dry-state characterization of TA-loaded β CD-Solu-NPs

Fourier transform infrared spectroscopy

The intermolecular interactions of the drug with the polymers were assessed by FTIR spectroscopy. FTIR analysis of TA, physical mixture, and the optimized formulation are shown in Figure 3 (A). The FTIR spectrum of the TA shows the characteristic peak at 3391.19 cm⁻¹ for OH stretching vibration, the peak observed at 2989.70 cm⁻¹ and 2951.07 cm⁻¹ for the C-H vibrations, the peak observed at 1706.06 cm⁻¹ indicating C=O stretching of aliphatic ketone, the peak at 1662.18 cm⁻¹ for the C=O of conjugated ketone present in TA. The strong peak observed at 1056.31 cm⁻¹ represents the C-F stretching of the halogenated ring present in the TA structure, which confirms the structure of TA. The IR spectra of the mixture of TA, βCD, and Soluplus show a peak at 3387.94 cm⁻¹ for the -OH stretching vibrations, and the peaks observed at 2942 cm⁻¹ and 2904.92 cm⁻¹ stands for the C-H stretching vibrations from TA and Soluplus, respectively. The peak at 1730.06 cm⁻¹ indicates the ester bond from Soluplus, and the peak at 1708.47 cm⁻¹ indicates the C=O for aliphatic ketones from TA. The peak present at 1660.26 cm⁻¹ confirms the presence of C=O from the conjugated ketone of TA. The strong C-C-O-C peak at 1024.98 cm⁻¹ represents ether linkage from βCD, and the peak observed at 1415.07 cm⁻¹ represents O-H bending vibrations from βCD. These results indicate the presence of TA, Soluplus, and βCD in the physical mixture without any significant interactions and confirm the physical compatibility between them. The formulation contains the TA nanoparticles enclosed in the βCD complex along with Soluplus, indicating the successful inclusion as a

result of the observance of the peak at 3396.37 cm⁻¹ representing the -OH of Soluplus or the peak observed at 3281.70 for -OH stretching from β CD, and the peak at 1021.16 for C-O stretching of the ether bond present in β CD. There were no other peaks from TA, indicating successful inclusion in the β CD matrix. Hence, using FTIR, preliminary confirmation of TA encapsulation was confirmed based on the characteristics of the functional peaks.

X-ray diffraction analysis (XRD)

XRD analysis of the nanomaterials was performed to evaluate their phase transition behavior. Figure 3 (B) illustrates the X-ray diffraction patterns of the drug, blank formulation, and freeze-dried TA-loaded βCD-Solu-NP nanosuspensions produced via solvent evaporation. The intact TA X-ray diffraction data revealed sharp peaks in the range of $2\theta = 9-24^{\circ}$. particularly at $2\theta = 9.95^{\circ}$, 14.59° and 24.79° , which are characteristic of the crystalline structure of the drug. The blank formulation displayed certain diffraction bands of the polymer, with sharp peaks at $2\theta = 9.71^{\circ}$ and 24.65° . The X-ray TA-loaded βCD-Solu-NPs pattern of demonstrated peak broadening and reduced peak intensity, indicating that TA was encapsulated within the polymers, resulting in semi-crystalline solid nanoparticles.

Differential scanning calorimetry (DSC) assessment

In the TA thermogram, a broad exothermic appeared at 291.71 °C, likely caused by moisture evaporation and polymer degradation, confirming its hygroscopic nature (Fig. 3 (C)). The glass transition temperature (Tg) exhibited a peak at 182.86 °C. The physical mixture showed a wide endothermic peak for βCD at 109.51 °C and a peak for TA at 288.43 °C, confirming compatibility, with a Tg of 176.01 °C relative to TA. The DSC thermogram of the lyophilized TAloaded BCD-Solu-NP formulation lacked a TA peak, indicating that TA was encapsulated in the NP matrix, while an endothermic peak at 162.85 °C confirmed complexation, along with a sharp endothermic peak suggesting crystalline properties, indicating a stable formulation compared to the plain pure drug TA. Additionally, a broad peak at 303.52 °C denoted moisture and degradation indicators.

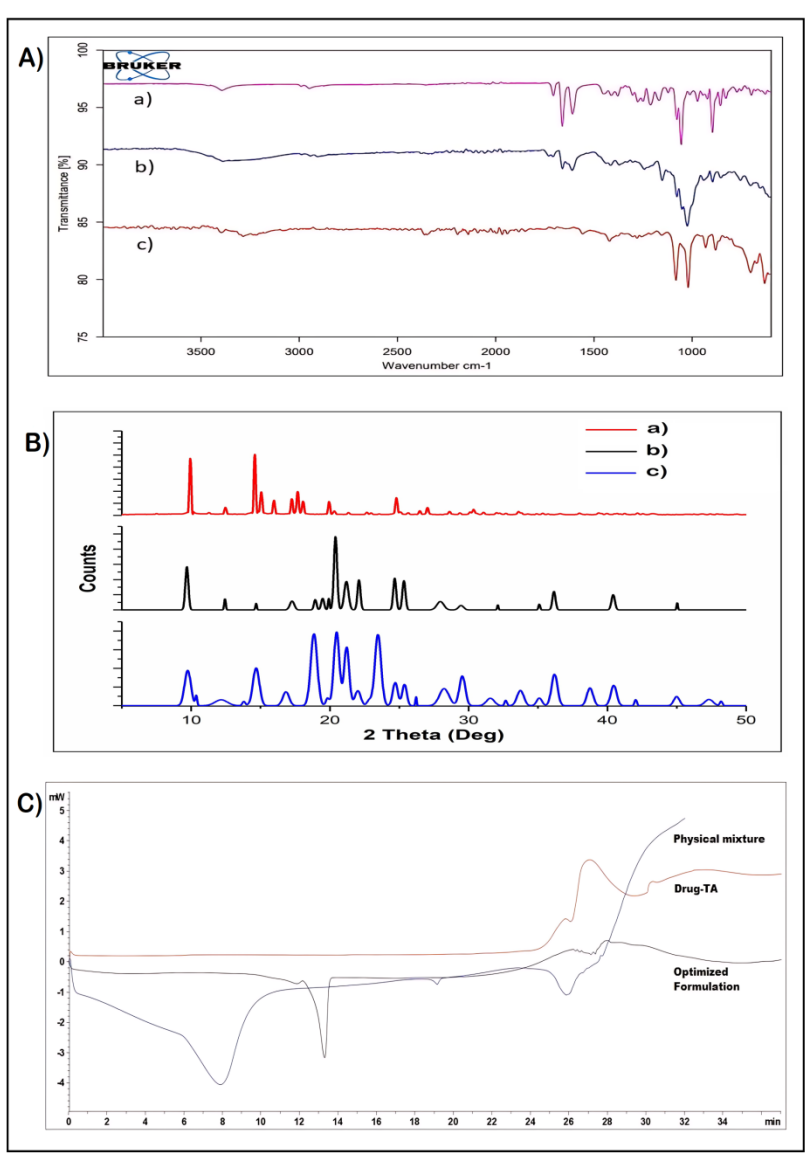


Figure 3: Dry state characterization of TA-loaded β CD-Solu-NPs, (A) FTIR spectra of a) TA-pure drug, b) physical mixture and c) TA-loaded β CD-Solu-NPs, (B) XRD diffractogram of a) TA-pure drug, b) blank formulation and c) TA-loaded β CD-Solu-NPs, and (C) DSC thermogram of a) TA-pure drug, b) physical mixture and c) TA-loaded β CD-Solu-NPs

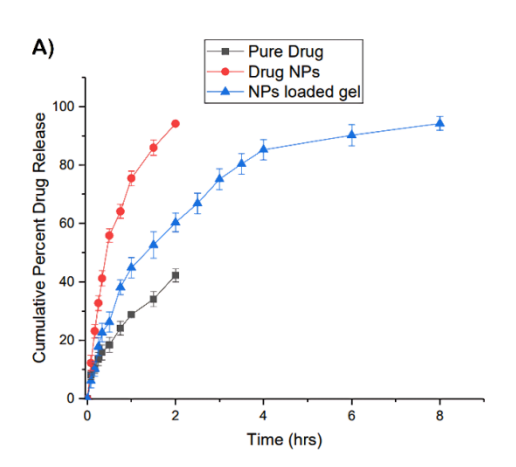
Release assessment – in vitro and diffusion kinetics study

Figure 4 illustrates the drug release profiles for pure TA, TA-loaded βCD-Solu-NPs, and xyloglucan-containing TA-loaded βCD-Solu-NPs. Pure TA released 42.21% of the drug after 2 h, while TA-loaded βCD-Solu-NPs yielded 94.12% in the same timeframe. The optimized formulation loaded in xyloglucan revealed 94.21% release over 8 h, in contrast to the pure TA and nanoparticles because of the properties of cyclodextrin, which enhance drug solubility, stability, and release. 5.38 The drug discharge mechanism was analyzed using kinetic models to evaluate release kinetics. Comparing the Higuchi

 $(R^2 = 0.9732)$, the zero-order $(R^2 = 0.8741)$ and the first-order $(R^2 = 0.9866)$ kinetic models, the plot obtained for the last model indicated the highest coefficient of linearity, suggesting that the first-order kinetic model closely matched the *in vitro* release. The Korsmeyer-Peppas equation showed significant linearity $(R^2 = 0.9748)$ between the log time and log cumulative percentage of TA released. The release exponent (n) and kinetic constant (k) were determined to be 0.4614 and 0.3079, respectively. The release exponents (n) for all formulations were <0.5, suggesting that matrix diffusion governs TA release and that quasi-Fickian diffusion is the main discharge principle.^{5,38}

Release assessment – ex vivo permeation

The relative *ex vivo* release characteristics of TA-loaded βCD-Solu-NPs in STF and pure TA across the dissected cornea of the goat are shown in Figure 4. The pure drug TA achieved total drug release (35.46%) after 2 h owing to its poor aqueous solubility. Conversely, the TA-loaded



βCD-Solu-NPs formulation displayed an extended release of up to 8 h (96.13%). The permeation data indicated that the final formulation batch exhibited steady-state diffusion coefficient (D), apparent coefficient permeability (Papp), and steady-state flux (Jss) of 1.22503 ± 0.002 (cm⁻² h⁻¹), 0.3771 ± 0.003 (cm⁻² h⁻¹), and 754.621 ± 1.1 (g cm⁻² h⁻¹), respectively.

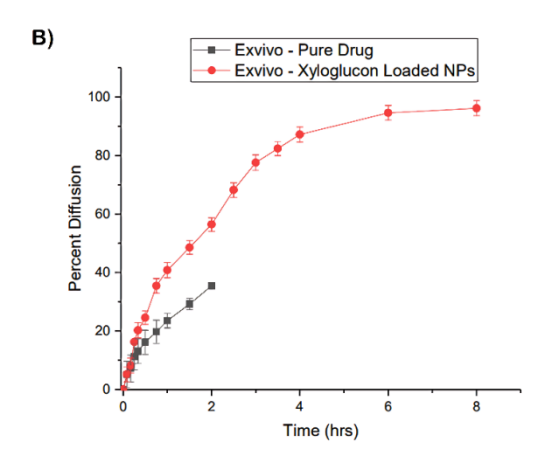


Figure 4: (A) *In-vitro* release profile of pure drug TA, TA-loaded βCD-Solu-NPs (Drug NPs) and xyloglucan containing TA-loaded βCD-Solu-NPs (NPs loaded gel), and (B) *Ex-vivo* permeation of pure drug TA (ex vivo - pure drug), and xyloglucan containing TA-loaded βCD-Solu-NPs (ex vivo - xyloglucan loaded NPs)

This study confirmed that nanoparticle encapsulation combined with a thermoresponsive gel system offers a viable method for ocular drug delivery, ensuring prolonged retention, controlled release, and enhanced permeation. This formulation strategy could potentially improve therapeutic efficacy, reduce dosing frequency, and enhance patient compliance with ophthalmic treatments.²³

Thermal gelation (in-situ gelling)

An initial assessment of the gel-forming properties of the processed xyloglucan was conducted to confirm the gel region. The conversion temperature for the sol-gel processes was measured as a function of concentration throughout the relevant range. The xyloglucan solution, comprising xyloglucan with 45% GRR in STF (pH 7.4), demonstrated reversible sol-gel transition properties. All prepared batches were assessed for their gelling capacity in STF at 37 °C. All batches were successfully gelled at physiological temperature, but exhibited concentration-dependent gelling ability (denoted by + in Table 5). Batch F2 showed superior gelling ability compared to F1 and F3, with F1 yielding less gelation and F3 demonstrating more

gelation, which may cause vision disturbance due to stickiness. The GFT values measured for the xyloglucan solution ranged from 28 °C to 33 °C. At this GFT, raw xyloglucan did not show gel formation, suggesting a relationship with the GRR. If the system gels at a temperature above physiological conditions, it may not convert to the gel form after application at the eye site. Conversely, if the gelling temperature is too low, the gel may gel during storage. The sol–gel transition was entirely reversible. After gelation under physiological conditions, formulation batches F1, F2, and F3 showed a positive effect on viscosity as the concentration of enzymatically degraded xyloglucan increased (Table 5). 36,39-40

Hen's egg test – chorioallantoic membrane study (HET-CAM test)

It is vitally important to assess potential irritation before administering ophthalmic products to humans. The irritation effect of TA-loaded βCD-Solu-NPs was assessed by the HET-CAM test. The HET-CAM assay involves evaluating, scoring, and standardizing features such as haemorrhage, vascular lysis, and coagulation at the site of application (Fig. 5). Following CAM exposure to 0.1N NaOH

(positive reference), which resulted in significant vascular damage and irritancy ratings of 12.0, the final ocular irritancy outcomes are given in Table 6. At the site of action, the negative control using 0.9% NaCl did not result in any coagulation, haemorrhage, or vessel damage in the CAM, and the same results were obtained for the optimized

formulation. The optimized batch, comprising TA-loaded β CD-Solu-NPs, produced a diminished irritancy score close to zero (0.45). This lower score indicated that the TA-loaded β CD-Solu-NPs were non-irritating, confirming their suitability for ophthalmic medication delivery.

Table 5 Xyloglucan composition (%w/w) and gelling capacity

]	Formulation batch	ies
	F1	F2	F3
GRR xyloglucan (%w/w)	1.5	2.5	3.5
Gelling capacity	+	++	+++
Viscosity (cP)	2900 ± 102	7310 ± 140	11621 ± 179

*+, ++, +++ a sign of gelling directly proportional to the concentration of xyloglucan (GRR), (n = 3 times)

Table 6
Ocular irritation study using the HET-CAM score test

	Score of ocular irritation								
Observed response	red response Optimised formulation		Positive control		Negative control				
			mulation		(0.1N NaOH)			(0.9% NaCl)	
Time (minutes)	0.5	2	5	0.5	2	5	0.5	2	5
Vessels lysis (A)	0	0	0	0	0	2	0	0	0
Haemorrhage (B)	0	0.1	0.1	0	0	3.5	0	0	0
Coagulation (C)	0	0.1	0.15	0	2.5	4	0	0	0
Cumulative response after 5 min (A+B+C)	0.45		12.0		0.0				

^{*} n = 3 times

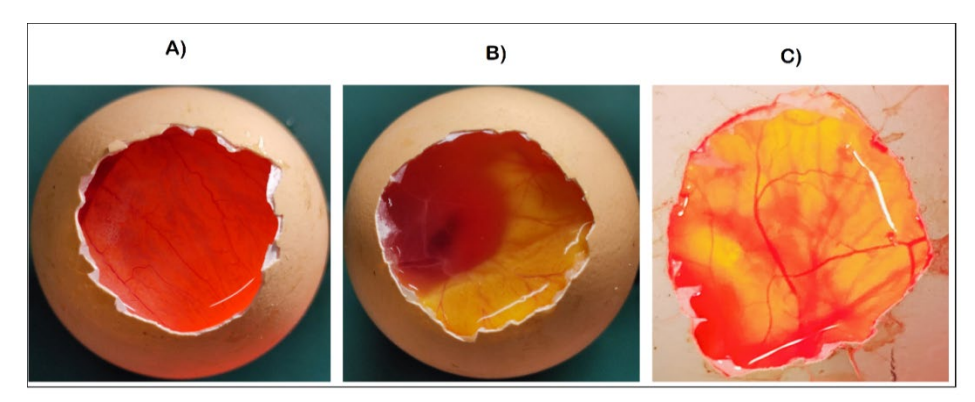


Figure 5: HET-CAM test results for ocular irritancy using (A) the optimized formulation, (B) negative and (C) positive controls

CONCLUSION

In this study, a solvent evaporation process combined with lyophilization was successfully employed to develop and characterize the TA-loaded βCD-Solu-NPs. This formulation illustrated improved corneal permeation, which was optimized using the response surface graph method (CCD) through a Quality by Design (QbD) approach, and indicated that the independent variables had a significant impact on

particle size, percentage encapsulation, surface charge, and PDI. In addition to solid-state assessment using FTIR, XRD, DSC, and surface morphology studies using SEM and HR-TEM, the developed nanoparticles were confirmed to have a nanospherical structure and a stable formulation. The optimized TA-loaded βCD-Solu-NP formulation, incorporated into a xyloglucan-based *in situ* gel, exhibited prolonged drug discharge

and non-irritating properties, as evidenced by the HET-CAM test.

ACKNOWLEDGEMENTS: Amneal Pharma, DSP Gokyo Food and Chemical, and BASF India are acknowledged for supplying gift samples of the medications TA, xyloglucan, and Soluplus, respectively.

REFERENCES

- ¹ G. Fang, X. Yang, Q. Wang, A. Zhang and B. Tang, *Mater. Sci. Eng. C.*, **127**, 112212 (2021), https://doi.org/10.1016/j.msec.2021.112212
- ² F. G. Senjoti, P. Timmins, B. R. Conway and A. M. Smith, *Eur. J. Pharm. Biopharm.*, **154**, 1 (2020), https://doi.org/10.1016/j.ejpb.2020.06.016
- ³ N. Morsi, D. Ghorab, H. Refai and H. Teba, *Int. J. Pharm.*, **506**, 57 (2016), https://doi.org/10.1016/j.ijpharm.2016.04.021
- ⁴ R. Nidhi, K. Dignesh and M. Manju, *J. Microencapsul.*, **14**, 1 (2018), https://doi.org/10.1080/02652048.2018.1425750
- ⁵ F. Li, Y. Wen, Y. Zhang, K. Zheng, J. Ban *et al.*, *Artif. Cells Nanomed. Biotechnol.*, **47**, 4097 (2019), https://doi.org/10.1080/21691401.2019.1683567
- M. L. Formica, G. U. U. Gamboa, L. I. Tártara, J. D. Luna, J. P. Benoit *et al.*, *Int. J. Pharm.*, **2019**, 118795 (2019), https://doi.org/10.1016/j.ijpharm.2019.118795
- ⁷ W. Yumei, L. Yuanyuan, L. Xinyue, D. Kebebe, Z. Bing *et al.*, *Asian J. Pharm. Sci.*, **14**, 1 (2019), https://doi.org/10.1016/j.ajps.2018.04.008
- ⁸ S. Noreen, S. A. Ghumman, F. Batool, B. Ijaz, M. Basharat *et al.*, *Int. J. Biol. Macromol.*, **152**, 1056 (2019), https://doi.org/10.1016/j.ijbiomac.2019.10.193
- U. D. Laddha and S. J. Kshirsagar, *J. Drug Deliv. Sci. Technol.*, 20, 102 (2020), https://doi.org/10.1016/j.jddst.2020.102112
- ¹⁰ S. Wu, C. Bian, X. Li, M. Chen, J. Yang *et al.*, *J. Control. Release*, **333**, 76 (2021), https://doi.org/10.1016/j.jconrel.2021.03.023
- ¹¹ S. Cohen, E. Lobel, A. Trevgoda and Y. Peled, *J. Control. Release*, **44**, 201 (1997), https://doi.org/10.1016/S0168-3659(96)01523-4
- ¹² W. Ma, H. Xu, C. Wang, S. Nie and W. Pan, *Int. J. Pharm.*, **350**, 247 (2008), https://doi.org/10.1016/j.ijpharm.2007.09.005
- ¹³ H. S. Mahajan, V. Tyagi, G. Lohiya, P. Nerkar, H. S. Mahajan *et al.*, *Drug Deliv.*, **7544**, 270 (2012), https://doi.org/10.3109/10717544.2012.704095
- ¹⁴ M. Shirakawa, K. Yamatoya and K. Nishinari, *Food Hydrocoll.*, **12**, 25 (1998), https://doi.org/10.1016/S0268-005X(98)00052-6
- ¹⁵ A. K. Andriola, S. Brun-Graeppi, C. Richard, M. Bessodes, D. Scherman *et al.*, *Carbohyd. Polym.*, **80**, 555 (2010),
- https://doi.org/10.1016/j.carbpol.2009.12.026
- ¹⁶ M. P. M. Núria Piqué and M. del Carmen Gómez-

Guillén, Int. J. Mol. Sci., 2018, 1 (2018), https://doi.org/10.3390/ijms19030673 ¹⁷ T. Cheng, J. Li, Y. Cheng, X. Zhang and Y. Qu, Res., (2019),Eve https://doi.org/10.1016/j.exer.2019.107805 ¹⁸ K. Jadhav, E. Kole, A. Abhang, S. Rojekar, V. Sugandhi et al., Dry. Technol., 2024, 1 (2024), https://doi.org/10.1080/07373937.2024.2437691 ¹⁹ K. Jadhav, E. Kole, R. Singh, S. K. Rout, R. K. Verma et al., Dry. Technol., 42, 1415 (2024), https://doi.org/10.1080/07373937.2024.2357181 ²⁰ Y. A. Sonar and H. S. Mahajan, *Mater. Technol.*, 125 (2020),https://doi.org/10.1080/10667857.2019.1659534 ²¹ P. Keshari, Y. Sonar and H. Mahajan, Mater. Technol., 34, 423 (2019),https://doi.org/10.1080/10667857.2019.1575535 ²² S. R. Pardeshi, M. P. More, C. V. Pardeshi, P. J. Chaudhari, A. D. Gholap et al., J. Drug Deliv. Sci. Technol.. 86. 104719 https://doi.org/10.1016/j.jddst.2023.104719 ²³ S. Alshehri, S. S. Imam, M. A. Altamimi, A. Hussain, F. Shakeel et al., AAPS PharmSciTech., 21, 1 (2020), https://doi.org/10.1208/s12249-020-01684-2 S. R. Pardeshi, N. S. Deshmukh, D. R. Telange, S. N. Nangare, Y. Y. Sonar et al., Futur. J. Pharm. Sci., 9 (2023), https://doi.org/10.1186/s43094-023-00551-8 ²⁵ E. Kole, K. Jadhav, N. Shirsath, P. Dudhe, R. K. Verma et al., J. Drug Deliv. Sci. Technol., 81, 104 (2023), https://doi.org/10.1016/j.jddst.2023.104261 ²⁶ Ameeduzzafar, J. Ali, A. Bhatnagar, N. Kumar and A. Ali, Int. J. Biol. Macromol., 65, 479 (2014), https://doi.org/10.1016/j.ijbiomac.2014.02.002 ²⁷ S. Mandpe, E. Kole, V. Parate, A. Chatterjee, A. Mujumdar et al., Dry. Technol., 41, 2418 (2023), https://doi.org/10.1080/07373937.2023.2251572 ²⁸ H. S. Mahajan and Y. A. Sonar, J. Polym. Res., 26, 8 (2019), https://doi.org/10.1007/s10965-019-1887-1 ²⁹ E. Kole, K. Jadhav, Z. Khan, R. K. Verma, A. Chatterjee et al., Futur. J. Pharm. Sci., 10, 156 (2024), https://doi.org/10.1186/s43094-024-00736-9 B. Mitu, M. Cerda and R. Hrib, ACS Omega, 8, 22203 (2023),https://doi.org/10.1021/acsomega.3c02579 ³¹ Y. Carri, M. T. Dom, A. Dom and S. Olivares, Microchem. J., 209, 112622 (2025),https://doi.org/10.1016/j.microc.2024.112622 A. Patil, S. Pardeshi, M. Kapase, P. Patil, M. More Drv.Technol., 42. al., 661 https://doi.org/10.1080/07373937.2023.2298778 ³³ C. V. Pardeshi, V. V. Agnihotri, K. Y. Patil, S. R. Pardeshi and S. J. Surana, Int. J. Biol. Macromol., 165, (2020),https://doi.org/10.1016/j.ijbiomac.2020.09.163 ³⁴ S. S. Patil, A. Bade and A. Tagalpallewar, J. Drug Technol., Sci. 46, 138 (2018),https://doi.org/10.1016/j.jddst.2018.05.010 O. M. Kolawole and M. T. Cook, Eur. J. Pharm.

Biopharm.,

184.

(2023),

https://doi.org/10.1016/j.ejpb.2023.01.007

- ³⁶ S. Ramasundaram, G. Saravanakumar, S. Sobha and T. H. Oh, *Int. J. Mol. Sci.*, **24**, 355 (2023), https://doi.org/10.3390/ijms24010355
- ³⁷ Z. Qin, B. Li, Q. Deng, Y. Wen, S. Feng *et al.*, *Molecules*, **29**, 658 (2024), https://doi.org/10.3390/molecules29030658
- ³⁸ M. S. Khan, P. R. Ravi, S. I. Mir and P. S. Rawat, *Int. J. Biol. Macromol.*, **233**, 123533 (2023), https://doi.org/10.1016/j.ijbiomac.2023.123533
- ³⁹ P. S. Rawat, P. R. Ravi, S. I. Mir, M. S. Khan, H. Kathuria *et al.*, *Pharmaceutics*, **15**, 405 (2023), https://doi.org/10.3390/pharmaceutics15020405
- ⁴⁰ P. M. W. Fatima, S. Dasankoppa, P. Solankiy, H. N. Sholapur, V. G. Jamakandi *et al.*, *Indian J. Heal. Sci. Biomed. Res.*, **2017**, 323 (2017), https://doi.org/10.4103/kleuhsj.kleuhsj